He et al. *Zool. Res.* 2026, 47(3): 676−690
https://doi.org/10.24272/j.issn.2095-8137.2025.329
https://cstr.cn/32248.14.zr.2025.329

ZR | Zoological Research

Article Open Access

Knockout of *hsd3b1* disrupts steroid hormone homeostasis and compromises gonadal development in zebrafish

Lijia He[1,3,#], Yaqing Wang[1,#], Zhiqin Ren[1], Chaofan Wang[1], Rui Qu[1], Houpeng Wang[1], Ding Ye[1,2], Zhengfang Chen[1,2,*], Yonghua Sun[1,2,3,*]

[1] *State Key Laboratory of Breeding Biotechnology and Sustainable Aquaculture*, *Hubei Hongshan Laboratory*, *Institute of Hydrobiology*, *Innovation Academy for Seed Design*, *Chinese Academy of Sciences*, *Wuhan*, *Hubei* 430072, *China*

[2] *School of Marine Biology and Fisheries*, *Hainan University*, *Haikou*, *Hainan* 570228, *China*

[3] *College of Advanced Agricultural Sciences*, *University of Chinese Academy of Sciences*, *Beijing* 100049, *China*

ABSTRACT

Steroid hormones are central regulators of gonadal differentiation, endocrine homeostasis, and reproductive function, with impaired steroid biosynthesis leading to metabolic dysfunction and reproductive disease. 3β-Hydroxysteroid dehydrogenase (3β-HSD), encoded by *HSD3B*, catalyzes the conversion of inactive Δ^5-3β-hydroxysteroid precursors into bioactive Δ^4-ketosteroids, representing a pivotal enzymatic step in steroidogenesis. In this study, CRISPR/Cas9-mediated disruption of *hsd3b1* in zebrafish produced pronounced endocrine and reproductive abnormalities, including aberrant gonadal development, interrenal hyperplasia, hyperpigmentation, and reduced fertility. Integrated RNA sequencing and targeted steroid hormone metabolomics further demonstrated extensive disruption of steroid hormone homeostasis in *hsd3b1* mutants, with attenuated sex-specific metabolic differences between males and females. These findings establish *hsd3b1* as an essential determinant of steroidogenic balance and gonadal development in zebrafish. The *hsd3b1* mutant line provides a robust and tractable vertebrate model for investigating how steroidogenic disruption reshapes reproductive development and endocrine physiology.

Keywords: Steroid hormone synthesis; Gonadal development; *hsd3b1*; Zebrafish

INTRODUCTION

Steroid hormones provide essential endocrine cues that coordinate gonadal development, sexual differentiation, and reproductive function across vertebrates (Cole et al., 2019; Deltourbe et al., 2025; Yang et al., 2024; Zhou et al., 2021). Their biosynthesis depends on a tightly regulated cascade of sequential enzymatic reactions within steroidogenic tissues. The initiation and progression of gonadal differentiation, gametogenesis, reproductive maturation, and the establishment and maintenance of secondary sexual characteristics are governed by precise spatiotemporal patterns of steroid hormone signaling (Li et al., 2024b; Zhang et al., 2025). Maintenance of endogenous steroid hormone homeostasis is therefore indispensable for normal gonadal development and reproductive competence. Disruption of this balance, whether due to dysregulation of key synthetic enzymes or exposure to exogenous environmental disruptors, can impair sex differentiation, compromise gametogenesis, and culminate in infertility (De Castro Assis et al., 2018; De Waal et al., 2009; Li et al., 2024a; Luzio et al., 2015; Zhang et al., 2024).

In humans, disruption of steroid hormone metabolism contributes to diverse endocrine and reproductive diseases. These conditions can arise from impaired steroidogenic enzyme function, abnormal hormone concentrations, or defects in hormone receptor signaling (Miller & Auchus, 2011). Among these conditions, congenital adrenal hyperplasia (CAH) comprises a group of autosomal recessive disorders caused by deficiencies in enzymes required for adrenal steroid hormone biosynthesis, resulting in reduced cortisol production (Simard et al., 2002, 2005). Major CAH subtypes include deficiencies in 21-hydroxylase, 11β-hydroxylase, 17α-hydroxylase/17,20-lyase, and 3β-hydroxysteroid dehydrogenase (3β-HSD) (Auer et al., 2023; Fraga et al., 2024). Among these disorders, 3β-HSD deficiency is caused by loss-of-function mutations in *HSD3B2*. Loss of 3β-HSD

This is an open-access article distributed under the terms of the Creative Commons Attribution Non-Commercial License (http://creativecommons.org/licenses/by-nc/4.0/), which permits unrestricted non-commercial use, distribution, and reproduction in any medium, provided the original work is properly cited.

Copyright ©2026 Editorial Office of Zoological Research, Kunming Institute of Zoology, Chinese Academy of Sciences

Received: 15 December 2025; Accepted: 20 April 2026; Online: 21 April 2026

Foundation items: This work was supported by the National Natural Science Foundation of China (32025037), Strategic Priority Research Program of the Chinese Academy of Sciences (CAS) (XDB0730300), Natural Science Foundation of Hubei Province (2025AFA053), Natural Science Foundation of Wuhan (2024040701010069), Science and Technology Special Fund of Hainan Province (ZDYF2024XDNY256), and Project of Cross-disciplinary Research Team (2024BBSA01) of the State Key Laboratory of Breeding Biotechnology and Sustainable Aquaculture to Y.S.

[#]Authors contributed equally to this work

*Corresponding authors, E-mail: yhsun@ihb.ac.cn; zhengfangchen@hainanu.edu.cn

activity disrupts steroid precursor conversion and can produce reproductive dysfunction and virilization of external genitalia in XX individuals, as well as undermasculinization and hypogonadism in XY individuals. Hyperpigmentation and salt wasting can also occur in both genotypic sexes, with variable clinical severity (Chen et al., 2021; Guran et al., 2020; Ladjouze et al., 2022; Mermejo et al., 2005; Moisan et al., 1999).

Steroidogenic defects have been characterized extensively in mice, and genetic models have clarified the functions of several enzymes required for steroid biosynthesis (Abou Nader & Boyer, 2021; Gonzalez Deniselle et al., 2016; Ikeda et al., 1994; Watters et al., 2021). Mouse mutant models have been generated for genes encoding key enzymes in the steroid synthesis pathway, including *Cyp11a1* (cholesterol side-chain cleavage enzyme, P450scc) (Tong et al., 2022), *Cyp17* (17α-hydroxylase/17,20-desmolase) (Secchi et al., 2021), *Cyp21a1* (21-hydroxylase) (Gotoh et al., 1994; Gotoh et al., 1988; Naiki et al., 2016), and *Hsd11b1* (11β-hydroxysteroid dehydrogenase-1) (Zhang et al., 2017). However, a mouse model that recapitulates 3β-HSD deficiency has not yet been established, likely because the expanded *Hsd3b* gene family, comprising *Hsd3b1–Hsd3b9*, makes it challenging to construct an effective loss-of-function model.

Zebrafish provide a tractable vertebrate system for dissecting steroidogenic regulation of endocrine and reproductive development. Gene-editing approaches have enabled the generation of mutants for multiple steroidogenic enzymes, including *cyp19a1a* (aromatase) (Lau et al., 2016; Tang et al., 2017; Wu et al., 2020; Yin et al., 2017), *cyp17a1* (17α-hydroxylase/17,20-lyase) (Yang et al., 2021; Zhai et al., 2018), *cyp17a2* (17α-hydroxylase) (Shi et al., 2022; Yang et al., 2024), *cyp21a2* (21-hydroxylase) (Eachus et al., 2017), *cyp11c1* (11β-hydroxylase) (Zhang et al., 2020b), *cyp11a1.2* (cholesterol side-chain cleavage enzyme, P450scc, also referred to as *cyp11a2)* (Li et al., 2020; Wang et al., 2022), and *cyp11a1.1* (also designated *cyp11a1*) (Zhang et al., 2025b). These models have demonstrated that steroidogenic enzymes are indispensable for gonadal differentiation, steroid hormone homeostasis, and gametogenesis. Nevertheless, the *in vivo* function of 3β-HSD within the steroid synthesis pathway remains unresolved. This enzyme, encoded by *hsd3b*, catalyzes the conversion of Δ^5-3β-hydroxysteroids, including pregnenolone and dehydroepiandrosterone, into Δ^4-ketosteroids, including progesterone and androstenedione, and thereby mediates an early obligatory step in the biosynthesis of active steroid hormones (Simard et al., 2005). Zebrafish possess two *hsd3b* homologs, with *hsd3b1* showing predominant gonadal expression and proposed functional orthology to human *HSD3B2* (Lin et al., 2015). These features make *hsd3b1* a suitable target for defining how 3β-HSD activity regulates steroidogenesis and gonadal development *in vivo*.

In this study, CRISPR/Cas9 gene editing was used to generate a zebrafish *hsd3b1* loss-of-function mutant. Notably, *hsd3b1*$^{-/-}$ zebrafish exhibited abnormal gonadal development, interrenal hyperplasia, hyperpigmentation, and reduced reproductive capacity. RNA sequencing (RNA-seq) combined with targeted steroid hormone metabolomics revealed extensive disruption of steroid hormone homeostasis in *hsd3b1*$^{-/-}$ mutants, accompanied by attenuated metabolic divergence between males and females. Together, these findings establish *hsd3b1* as a critical regulator of steroid biosynthesis and reproductive development in zebrafish.

MATERIALS AND METHODS

Fish and maintenance

All experiments were performed using AB strain zebrafish. Zebrafish were maintained under standard conditions as described previously (Kimmel et al., 1995) at the China Zebrafish Resource Center of the National Aquatic Biological Resource Center (CZRC-NABRC, Wuhan, China, http://zfish.cn). All zebrafish procedures complied with the Zebrafish Usage Guidelines of the China Zebrafish Resource Center (CZRC) and were approved by the Institutional Animal Care and Use Committee of the Institute of Hydrobiology, Chinese Academy of Sciences (approval no.: IHBLL2024076).

Quantitative real-time polymerase chain reaction (qPCR)

Total RNA was extracted from tissues of zebrafish at 3 months post-fertilization (mpf) using a FastPure Cell/Tissue Total RNA Isolation Kit (Cat. RC101-01, Vazyme, China) following the provided procedures. cDNA was synthesized from purified RNA using HiScript III All-in-one RT SuperMix Perfect for RT-PCR (Cat. R333, Vazyme, China) following the manufacturer's protocols. qPCR was performed using Taq Pro Universal SYBR RT-PCR Master Mix (Cat. Q712, Vazyme, China) and SYBR Green Supermix (Cat. 172-5124, Bio-Rad, China) on the Bio-Rad CFX96 Real-Time PCR Detection System. Expression values were calculated using the $2^{-\Delta\Delta CT}$ method and normalized to *β*-actin. The expression in the control sample was further normalized to 1. Primers used for RT-PCR are listed in Supplementary Table S1.

Generation and identification of *hsd3b1* mutants

The *hsd3b1* gene (ENSDARG00000069926) was disrupted using CRISPR/Cas9-mediated mutagenesis with zebrafish codon-optimized Cas9 (Deng et al., 2026; Zhang et al., 2020a). Briefly, a single-guide RNA (sgRNA) targeting the first exon of *hsd3b1* was designed using the online CRISPRscan platform (http://www.crisprscan.org/) (Moreno-Mateos et al., 2015). The target sequence was GCTGGTTCGACT GTTGCTGA*AGG*, with AGG serving as the protospacer-adjacent motif (PAM). Cas9 mRNA was synthesized using a T3 mMESSAGE mMACHINE mRNA Transcription Synthesis Kit (AM1344, Thermo Fisher Scientific, USA), with pCS2-nzcas9n (plasmid #CZP12, CZRC) as the DNA template. The sgRNA was synthesized using a TranscriptAid T7 High Yield Transcription Kit (K0441, Thermo Fisher Scientific, USA) according to the manufacturer's instructions. A 1 nL mixture containing Cas9 mRNA (400 ng/μL) and sgRNA (50 ng/μL) was co-injected into the animal pole of one-cell-stage zebrafish embryos. To confirm the mutation, genomic DNA was extracted from tail fins at 2 mpf, and the target region was amplified by PCR and sequenced. Primers used for sgRNA synthesis and target-site amplification are listed in Supplementary Table S1.

Enzyme-linked immunosorbent assay (ELISA)

Three wild-type (WT) and three *hsd3b1*$^{-/-}$ zebrafish at 3 mpf were euthanized with MS-222 (tricaine, Sigma-Aldrich, USA, >200 mg/L). Whole-body samples were transferred to grinding tubes containing magnetic beads, diluted with 1×phosphate-buffered saline (PBS, pH 7.2–7.4) at a 1:9 (w/v) ratio, and homogenized using a tissue homogenizer (Tissuelyser-24L, Jingxin, China). Protein concentrations in the homogenates were determined using a BCA protein assay kit (ADS-W-

SP002-48, AIDISHENG, China). Hsd3b1 and Hsd3b2 activities and the concentrations of 11-ketotestosterone and 17α,20β-dihydroprogesterone were quantified using commercial ELISA kits (MM-1525F2, MM-1534F1, MM-927244O2, and MM-1027Z2, China, respectively) according to the manufacturer's instructions.

Measurement of body weight and body length

Adult *hsd3b1*$^{+/-}$ males and females were crossed, and their resulting offspring were reared to adulthood and genotyped. Zebrafish at 4 mpf were anesthetized using MS-222 (150–200 mg/L). Body length was measured from the snout to the end of the caudal peduncle using a ruler with 0.1 cm precision. Before body weight measurement, excess surface moisture was gently removed with absorbent paper, and each fish was weighed using a balance with 0.0001 g precision.

Sampling and histological analysis

Zebrafish were euthanized by MS-222 and imaged using fixed camera parameters (Canon EOS 700D, Japan). Whole fish were then fixed in Bouin's fixative for 24 h before tissue processing. After standard histological preparation, samples were embedded in paraffin and sectioned at 2 μm using a microtome (HM340E, Thermo Scientific, USA). Sections were stained using a Hematoxylin and Eosin (H&E) High-Definition Permanent Staining Kit (G1076, Servicebio, China), examined and imaged under a microscope (Olympus BX53, Japan), or scanned using the Aperio VERSA system (Leica, Germany).

Single-molecule fluorescence *in situ* hybridization (smFISH)

Whole-mount smFISH was performed on zebrafish tissues fixed overnight in 4% paraformaldehyde (PFA) at 4°C, followed by hybridization as described in recent studies (Ren et al., 2024; Su et al., 2025; Wang et al., 2023). At least five probe pairs were designed for each target gene. After fixation, samples were washed three times in PBST (1×PBS containing 0.1% Tween 20, Sigma-Aldrich, USA) for 5 min per wash and permeabilized with 10 μg/mL proteinase K for 20 min. Samples were then washed three times with SSCT (20×saline-sodium citrate containing 0.1% Tween 20, Sigma-Aldrich, USA) for 5 min per wash and incubated with probes overnight at 37°C. After four washes, samples were incubated with labeled hairpins at room temperature for 4 h in the dark to initiate hybridization chain reaction (HCR). Unbound hairpins were removed by washing with SSCT, and samples were stained with 1 μg/mL 4',6-diamidino-2-phenylindole (DAPI) for 30 min before mounting in VECTASHIELD® mounting medium (Vector Laboratories, USA). Confocal images were acquired using a laser-scanning confocal inverted microscope (Leica SP8, Germany) equipped with a 63× oil-immersion objective and processed with LAS X Office software (https://www.leica-microsystems.com.cn/cn/c/gl/las-x-software-registration/).

Immunofluorescence (IF)

IF was performed as described in recent studies from this group (Chen et al., 2024; Ye et al., 2023). For whole-mount IF, zebrafish gonads were fixed in 4% PFA overnight at 4°C. For section IF, zebrafish gonads were fixed in 2% PFA at room temperature for 2 h and then sequentially equilibrated in 5%, 8%, 12%, 16%, and 20% sucrose for 30 min at each concentration. Samples were embedded in optimal cutting temperature (OCT) medium and cryosectioned at 12 μm using a CM5030 cryostat (Leica, Germany). Sections were washed three times (5 min each) with PBSBDT buffer containing 2% bovine serum albumin (BSA), 1% dimethyl sulfoxide (DMSO), and 0.1% Triton X-100 in PBS, and blocked in PBSBDT for 2 h at room temperature. After blocking, sections were incubated overnight at 4°C with primary antibodies diluted in PBSBDT, followed by incubation with anti-rabbit Alexa Fluor 488 secondary antibody (RRID: AB_2535792, Molecular Probes, USA) for 2 h at room temperature. Sections were mounted with VECTASHIELD® mounting medium. Confocal images were acquired using a laser-scanning confocal inverted microscope (Leica SP8, Germany) equipped with a 63× oil-immersion objective and processed using LAS X Office software.

RNA-seq and analysis

Zebrafish were euthanized by MS-222 at 3 mpf, and gonads were dissected from three independent individuals per group, representing three biological replicates. Each gonad was processed separately. Gonads were immersed in RNA keeper at 4°C overnight to allow complete reagent infiltration and then stored at −80°C. RNA extraction and sequencing were performed by the Analysis and Testing Center at the Institute of Hydrobiology, Chinese Academy of Sciences. Libraries were sequenced on the Illumina NovaSeq X Plus platform (USA) to generate 150 bp paired-end (PE) reads. High-quality clean reads were aligned to zebrafish reference transcripts derived from the GRCz11 genome assembly (Ensembl release 97). Differential expression analysis was performed using DESeq2 (Love et al., 2014), and genes with an adjusted $P<0.05$ were defined as differentially expressed genes (DEGs). Gene Ontology (GO) enrichment analysis of DEGs was performed and visualized using ClusterProfiler v.4.0 (Wu et al., 2021).

Determination and analysis of steroid hormone content

Zebrafish at 4 mpf were euthanized by MS-222, with six fish included in each group. After body length measurement, fish were transferred into centrifuge tubes, frozen overnight at –80°C, and lyophilized for 24 h using a cryogenic freeze dryer. Dry weight was then recorded. Steroid hormone extraction was performed by Wuhan Metware Metabolism Co., Ltd. (China). A 400 μL aliquot of steroid internal standard extraction solution, consisting of deuterated testosterone in methanol (25 ppb; CAS 77546-39-5), was added to each sample tube. Samples were vortexed at 2 500 r/min for 10 min at room temperature, sonicated for 15 min using a cell disruptor, incubated on ice for 10 min, and centrifuged at 12 000 r/min for 5 min at 4°C in a refrigerated centrifuge. A 370 μL aliquot of supernatant was transferred to a new tube and concentrated to dryness at –20°C. The dried extract was reconstituted in 100 μL of reconstitution solvent, vortexed for 3 min, and centrifuged at 12 000 r/min for 5 min at 4°C. The supernatant was collected in injection vials, stored at –20°C, and subjected to liquid chromatography-tandem mass spectrometry (LC-MS/MS). Information on reference standards used for LC-MS/MS is provided in Supplementary Table S3.

Data acquisition was performed using ultra-performance liquid chromatography (UPLC) (ExionLC™ AD) and MS/MS (QTRAP® 6500+). UPLC separation was conducted on a Phenomenex Kinetex C18 column. The mobile phases consisted of 30% acetonitrile/water containing 0.04% acetic acid (A) and 50% acetonitrile/isopropanol containing 0.04% acetic acid (B). The gradient started at 5% B (0–1.0 min), increased to 90% B (1.0–10 min), was maintained at 90% B (10–12.5 min), and finally returned to 5% B (12.6–15 min).

The flow rate was 0.35 mL/min, the column temperature was 40°C, and the injection volume was 5 μL. MS was operated in positive ion mode (ion source type, Turbo spray; ion source temperature, 550°C; ion spray voltage, 5 500 V; curtain gas pressure, 35.0 psi). The MS data were processed using Analyst v.1.6.3 and MultiQuant v.3.0.3.

Differential metabolites were screened according to absolute $\log_2$fold-change (FC) among significantly regulated metabolites between groups. Identified metabolites were annotated using the Kyoto Encyclopedia of Genes and Genomes (KEGG) Compound database and then mapped to the KEGG Pathway database. Pathways containing significantly regulated metabolites were analyzed by metabolite set enrichment analysis (MSEA), with significance determined using *P*-values from a hypergeometric test. Plots were generated using ComplexHeatmap v.2.12.0 and pandas v.0.23.4 (Kanehisa & Goto, 2000; Nouri et al., 2020).

Whole-mount *in situ* hybridization (WISH)

Gene-specific fragments were amplified by PCR and used as templates to synthesize digoxigenin-labeled antisense RNA probes. Embryos at 5 days post-fertilization (dpf) were fixed in 4% PFA for 12 h at 4°C and transferred to 100% methanol for long-term storage at −20°C. WISH was performed using the digoxigenin-labeled antisense RNA probes as described previously (Thisse & Thisse, 2008; Zhang et al., 2020b). Primers used for probe synthesis are listed in Supplementary Table S1.

Hydrocortisone treatment

Chorions were removed from *hsd3b1*$^{-/-}$ and WT embryos at 1 dpf. Embryos were then cultured by immersion in 0.3×Danieau's buffer containing 100 nmol/L hydrocortisone (H110523, Aladdin, China), and the working solution was replaced daily. Untreated siblings were used as controls. At 5 dpf, embryos from treatment and control groups were subjected to WISH using *cyp21a2* as a probe to label interrenal tissue. Each embryo was imaged, and the area of *cyp21a2*-positive interrenal tissue was quantified using ImageJ (https://imagej.net/ij/). Embryos were genotyped individually. Data were analyzed and plotted using GraphPad Prism v.10.4.0 (https://www.graphpad.com/updates/prism-10-4-0-release-notes).

Statistical analysis

Data analysis and graph generation were performed using GraphPad Prism v.10.4.0. Steroid hormone levels were analyzed using two-way analysis of variance (ANOVA), and the corresponding results are presented in Supplementary Tables S4–S18. All other datasets were analyzed using unpaired two-tailed Student's *t*-test. Data are presented as mean±standard deviation (SD). Statistical significance was denoted as follows: ns: not significant; *: P<0.05; **: P<0.01; ***: P<0.001; ****: P<0.0001.

RESULTS

Expression of *hsd3b1/2* and generation of *hsd3b1* mutants in zebrafish

qPCR analysis was first performed to define the tissue distribution of *hsd3b1* and *hsd3b2* in WT zebrafish. Both genes were detected across multiple tissues, including testes, ovaries, and head kidneys (Figure 1A; Supplementary Figure S1), with *hsd3b1* showing particularly strong expression in the testis (Supplementary Figure S1). Given the close relevance of gonadal and interrenal steroidogenic tissues to 3β-HSD deficiency, smFISH experiments were used to further resolve *hsd3b1/2* expression in the head kidney and gonads. Notably, *hsd3b1* was detected in the head kidney of both females and males (Figure 1B). In the gonads, *hsd3b1* produced strong signals in the testis, whereas *hsd3b2* showed only weak expression in the ovary (Figure 1C1–4). More importantly, testicular *hsd3b1* expression was almost completely co-localized with *insl3* (Figure 1C5–8), a specific marker of Leydig cells (Ivell et al., 2013). This expression pattern indicated enrichment of *hsd3b1* in the principal steroidogenic cell population of the testis (Zirkin & Papadopoulos, 2018).

To further investigate the functional role of *hsd3b1* in zebrafish gonads, *hsd3b1* mutant lines were generated using CRISPR/Cas9-mediated genome editing. A guide RNA (gRNA) targeting the first exon of *hsd3b1* was designed and validated for editing activity (Supplementary Figure S2). PCR amplification and sequencing of the target region identified three distinct mutant alleles carrying –6 bp, –19 bp, and +8 bp indels (Figure 1D). The –19 bp frameshift allele was selected for subsequent propagation because it introduced a premature termination codon and was predicted to disrupt protein structure and functional domains, thereby abolishing *hsd3b1* function (Figure 1E) (Waterhouse et al., 2018). ELISA-based quantification further showed that Hsd3b1 enzyme activity was significantly reduced in the *hsd3b1*$^{-/-}$ mutants compared with WT fish, confirming successful generation of the *hsd3b1* loss-of-function line (Figure 1F).

***hsd3b1* mutants exhibit reduced reproductive capacity**

To assess the functional role of *hsd3b1* in zebrafish development and reproduction, F1 heterozygotes were intercrossed to generate F2 progeny. Genotyping of F2 offspring revealed a WT:heterozygous:homozygous mutant ratio of approximately 1:2:1 (n=40 WT, n=91 *hsd3b1*$^{+/-}$, n=48 *hsd3b1*$^{-/-}$), consistent with Mendelian inheritance and indicating that homozygous mutants survived to sexual maturity. WT and *hsd3b1*$^{-/-}$ adults showed marked differences in body coloration. WT males exhibited light yellow pigmentation, whereas WT females displayed blue-gray coloration; in contrast, both male and female *hsd3b1*$^{-/-}$ fish showed intensified yellow pigmentation relative to WT counterparts (Figure 2A1–A8). No significant difference in body weight was observed between WT and *hsd3b1*$^{-/-}$ fish (Supplementary Figure S3A, B), but *hsd3b1*$^{-/-}$ mutants were significantly longer than WT fish (Supplementary Figure S3C, D).

Reproductive assessment revealed pronounced fertility impairment in both sexes. When *hsd3b1*$^{-/-}$ males (n=3) were paired with WT females at a ratio of one *hsd3b1*$^{-/-}$ male to two WT females, mutant males showed markedly reduced sperm-release frequency relative to WT males (three vs. nine times over 10 trials) and prolonged intervals between sperm-release events (9±0 vs. 3.4±0.7 days, P<0.0001; Figure 2B). Similarly, *hsd3b1*$^{-/-}$ females showed severe reproductive defects. Initial assays at 3 mpf showed that only 33.3% of *hsd3b1*$^{-/-}$ females spawned spontaneously (four spawners among 12 tested females; Figure 2C), prompting subsequent assessment at 5 mpf. When *hsd3b1*$^{-/-}$ females (n=3 females) were paired with WT males at a ratio of one *hsd3b1*$^{-/-}$ female to two WT males, mutant females produced significantly fewer eggs per spawning event than WT females (65±59 vs. 227±81 eggs, P<0.0001) (Figure 2D). In addition, 16.7% of *hsd3b1*$^{-/-}$ females failed to ovulate throughout their lifespan despite

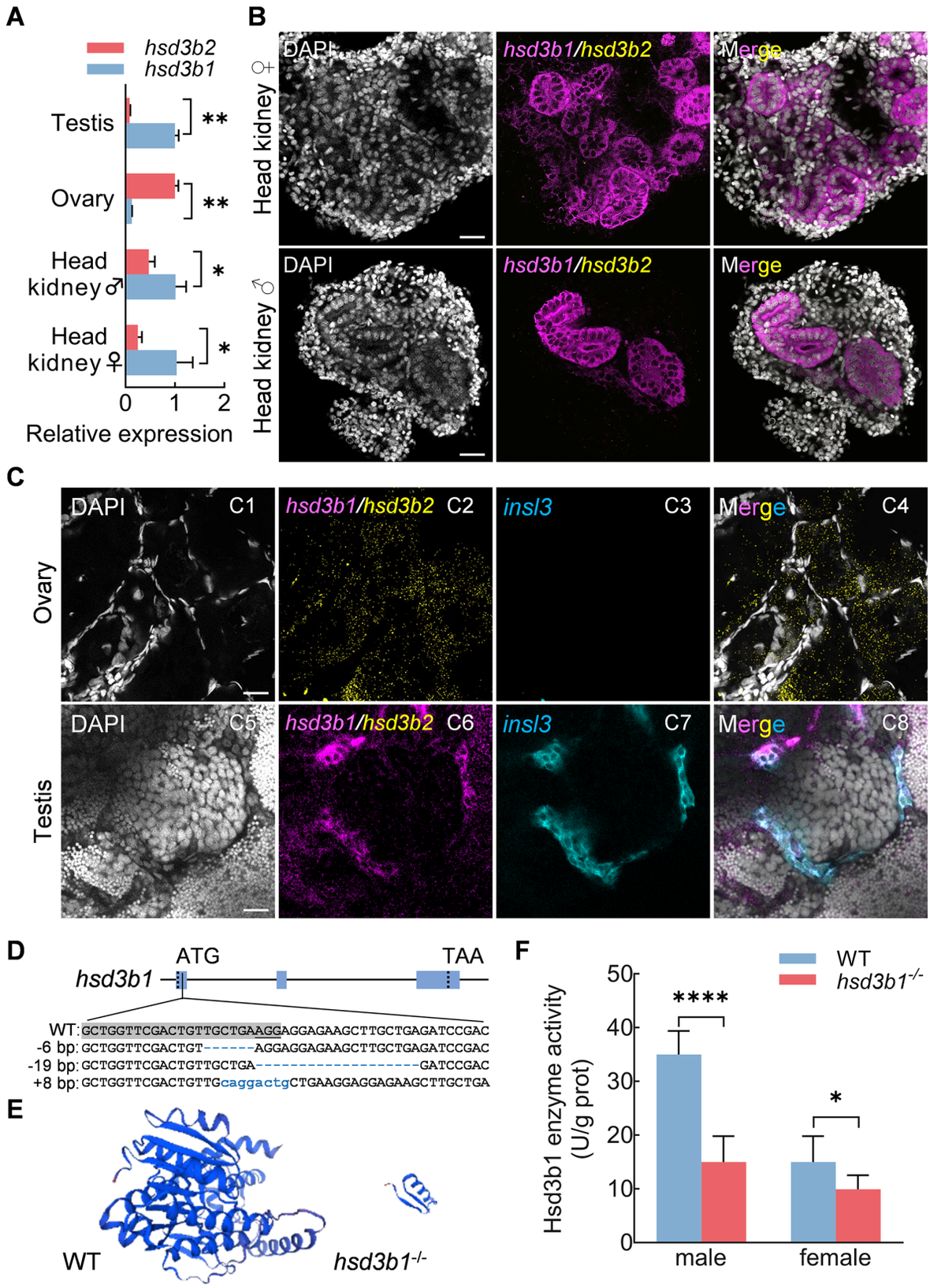


Figure 1 Expression patterns of *hsd3b1/2* and generation of *hsd3b1* mutants

A: qPCR analysis of *hsd3b1* and *hsd3b2* transcription levels in female and male gonads and head kidneys. B: smFISH detection of *hsd3b1* and *hsd3b2* expression in the head kidneys of 3 mpf zebrafish. Scale bars: 20 μm. C: smFISH detection of *hsd3b1*, *hsd3b2*, and *insl3* expression in 3 mpf zebrafish gonads. Scale bars: 20 μm. D: Schematic of *hsd3b1* gene structure and CRISPR/Cas9-induced mutations. The CRISPR target sequence in the WT allele is shaded in gray, and the protospacer adjacent motif (PAM) is underlined. Mutation sites are shown in blue. Three mutation types were generated, and the 19 bp deletion allele was selected for subsequent experimental validation. E: Predicted structures of WT and mutant Hsd3b1 proteins. F: Hsd3b1 enzymatic activity in WT and *hsd3b1*$^{-/-}$ zebrafish. Data are presented as mean±SD. Unpaired two-tailed Student's *t*-test was used in panels A, F. ns: Not significant; *: P<0.05; **: P<0.01; ***: P<0.001; ****: P<0.0001.

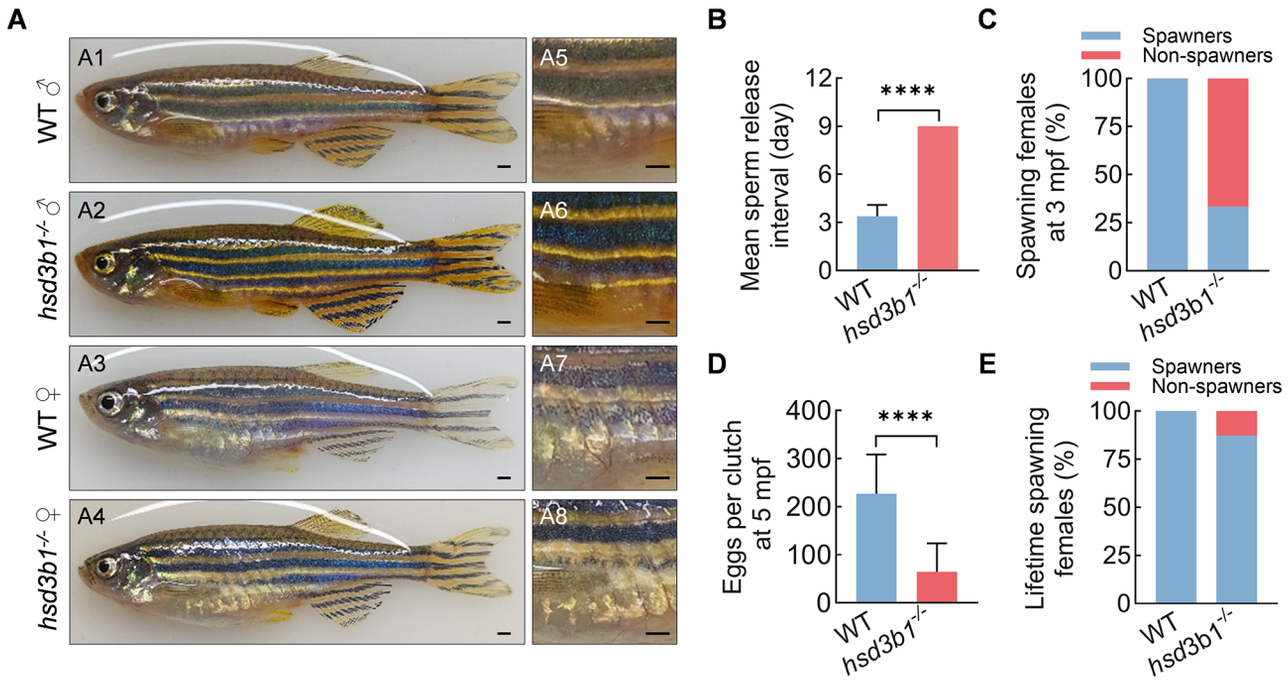


Figure 2 Growth characteristics and reproductive capacity of WT and *hsd3b1* mutant zebrafish

A: Comparison of body coloration between male and female zebrafish in WT and *hsd3b1*$^{-/-}$ groups. Scale bar: 0.1 cm. B: Comparison of intervals between sperm-release events in 3 mpf WT and *hsd3b1*$^{-/-}$ males. C: Percentage of females capable of spontaneous spawning in WT and *hsd3b1*$^{-/-}$ groups at 3 mpf. D: Comparison of egg number per clutch after mating of 5 mpf WT or *hsd3b1*$^{-/-}$ females with WT males. E: Percentage of females with lifetime spawning failure in WT and *hsd3b1*$^{-/-}$ groups. Data are presented as mean±SD. Unpaired two-tailed Student's *t*-test was used in panels B, D. ns: Not significant; *: P<0.05; **: P<0.01; ***: P<0.001; ****: P<0.0001

repeated manual extrusion attempts (two non-spawners among 12 tested females; Figure 2E). These results indicate that *hsd3b1* is required for normal reproductive performance in zebrafish and that *hsd3b1* deficiency impairs fertility in both males and females.

hsd3b1 mutants exhibit gonadal developmental abnormalities

To determine whether the impaired fertility observed in *hsd3b1*-deficient zebrafish reflected defective gonadal development, serial H&E staining was performed on gonads from F2 WT and *hsd3b1*$^{-/-}$ zebrafish at successive developmental stages. In females, WT ovaries at 60 dpf were enlarged and contained abundant stage III oocytes, including some oocytes approaching stage IV, whereas *hsd3b1*$^{-/-}$ ovaries were smaller and contained oocytes with reduced diameters, with stage II oocytes predominating (Figure 3A–B1). At 75 dpf, WT ovaries were dominated by stage IV oocytes, whereas *hsd3b1*$^{-/-}$ ovaries still contained abundant stage II and III oocytes despite the emergence of stage IV oocytes (Figure 3C–D1). At 90 dpf, WT oocytes continued to expand and reached full maturation, whereas *hsd3b1*$^{-/-}$ ovaries still retained a higher proportion of immature oocytes, although the developmental difference relative to WT ovaries had narrowed (Figure 3E–F1). These results indicate that *hsd3b1* deficiency delays ovarian development, with partial attenuation of the delay during later development. In males, histological analyses revealed significant Leydig cell hyperplasia in *hsd3b1*$^{-/-}$ testes. Compared with WT testes, which were primarily populated by germ cells and contained sparse Leydig cells, *hsd3b1*$^{-/-}$ testes exhibited markedly expanded Leydig cell populations and substantially reduced numbers of mature spermatozoa (Figure 3G–L1). Collectively, these findings demonstrate that *hsd3b1* deficiency disrupts gonadal development in zebrafish by delaying ovarian maturation and disturbing testicular Leydig cell-germ cell homeostasis.

hsd3b1 mutants exhibit a slowdown in both male and female gametogenesis

To define how *hsd3b1* deficiency alters gonadal development at the molecular level, transcriptome profiling was performed on F2 zebrafish gonads at 3 mpf across four groups: WT testis, WT ovary, *hsd3b1*$^{-/-}$ testis, and *hsd3b1*$^{-/-}$ ovary, with three biological replicates per group. Principal component analysis (PCA) demonstrated clear separation among the four groups in both two-dimensional (2D) and three-dimensional (3D) plots, indicating distinct transcriptomic profiles across the four experimental groups (Supplementary Figure S4A, B).

In the testes, comparison of *hsd3b1*$^{-/-}$ and WT samples identified 576 DEGs, including 418 up-regulated and 158 down-regulated genes (Figure 4A). qPCR validation of selected DEGs supported the reliability of the RNA-seq data (Figure 4G). GO enrichment analysis showed that up-regulated genes were significantly associated with extracellular matrix and extracellular space categories (Figure 4B), which are closely related to the establishment of testicular structure in zebrafish (Uribe et al., 2014). These genes are involved in intercellular signaling, nutrient exchange, and the steroidogenic microenvironment of the testis (Zirkin & Papadopoulos, 2018). Enrichment of calcium ion-related pathways and oxidoreductase activity further suggested remodeling of steroidogenic and redox-associated processes after loss of 3β-HSD activity. In contrast, down-regulated genes were enriched in pathways related to mitotic regulation, negative regulation of apoptosis, chromatin organization, nucleosome assembly, and chromatin remodeling (Figure 4C), indicating reduced proliferative and differentiation activity in spermatogenic cells. These transcriptomic changes were consistent with the histological

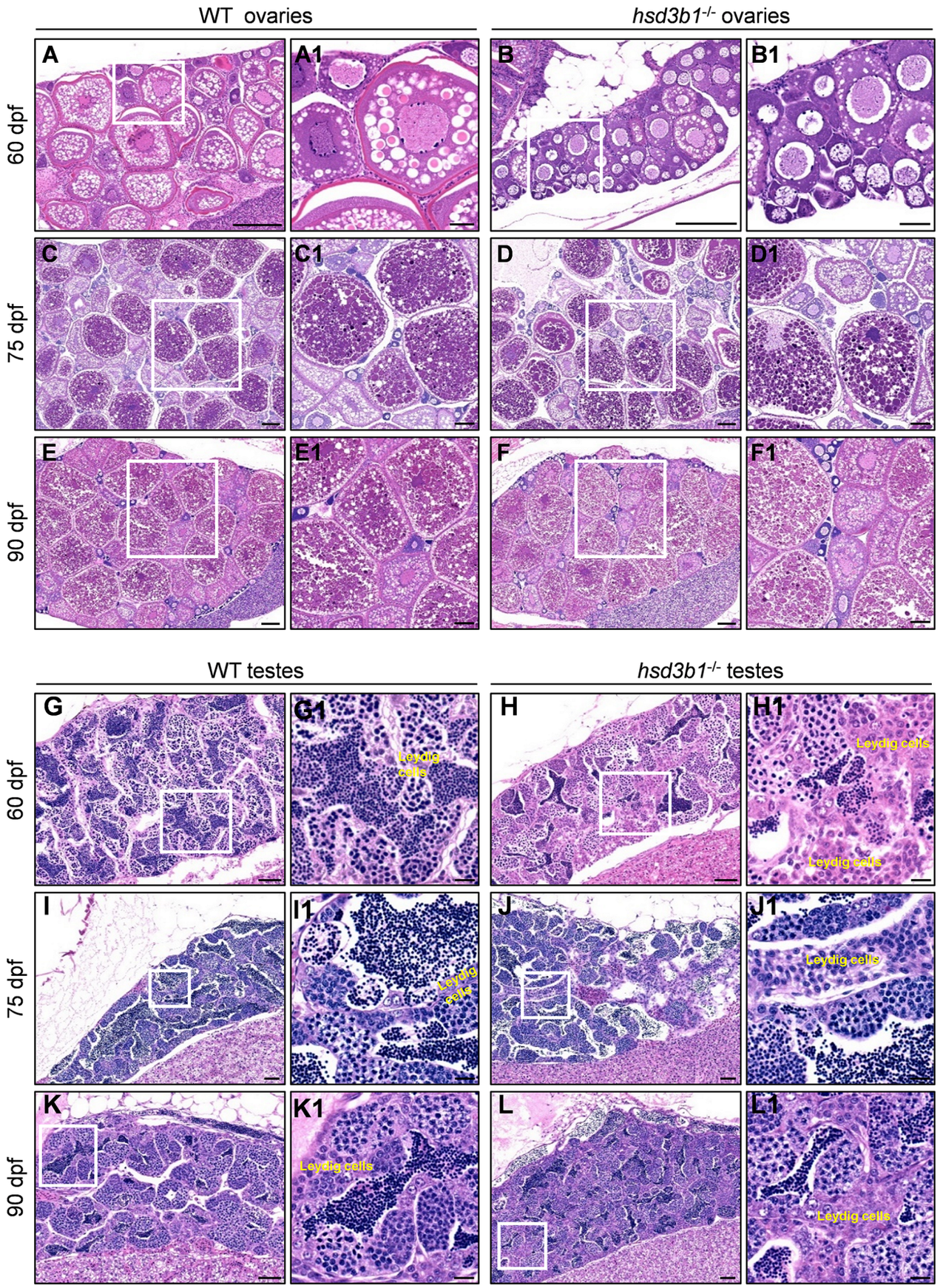


Figure 3 H&E-stained sections of WT and *hsd3b1*$^{-/-}$ gonads

A–F1: Ovarian H&E staining of WT and *hsd3b1*$^{-/-}$ zebrafish at 60, 75, and 90 dpf. Left panel shows overall developmental status of the ovary (scale bar: 50 μm), and right panel shows a magnified view of the boxed regions (scale bar: 10 μm). G–L1: Testicular H&E staining of WT and *hsd3b1*$^{-/-}$ zebrafish at 60, 75, and 90 dpf. Left panel shows overall developmental status of the testis (scale bar: 50 μm), and right panel shows a magnified view of the boxed regions (scale bar: 10 μm). Increased Leydig cell abundance was observed in *hsd3b1*$^{-/-}$ testes compared with WT testes.

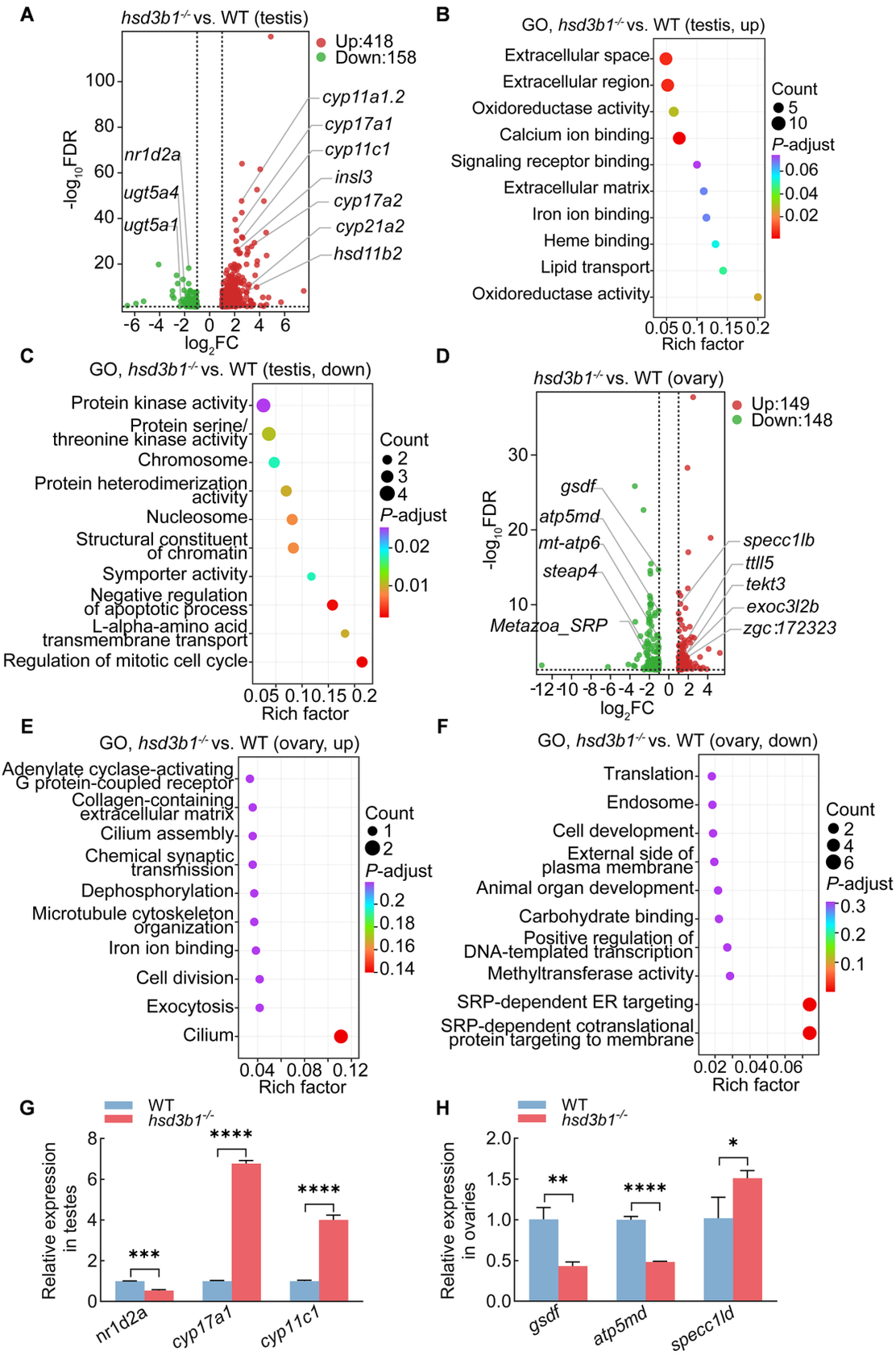


Figure 4 RNA-seq analysis of WT and *hsd3b1*$^{-/-}$ gonads

A: Differential gene expression trends in the testes of WT and *hsd3b1*$^{-/-}$ zebrafish. B: GO enrichment analysis of up-regulated genes in WT and *hsd3b1*$^{-/-}$ testes. C: GO enrichment analysis of down-regulated genes in WT and *hsd3b1*$^{-/-}$ testes. D: Differential gene expression trends in the ovaries of WT and *hsd3b1*$^{-/-}$ zebrafish. E: GO enrichment analysis of up-regulated genes in WT and *hsd3b1*$^{-/-}$ ovaries. F: GO enrichment analysis of down-regulated genes in WT and *hsd3b1*$^{-/-}$ ovaries. G–H: qPCR validation of selected RNA-seq DEGs in testes and ovaries. Data are presented as mean±SD. Unpaired two-tailed Student's *t*-test was used in panels G, H. ns: Not significant; *: P<0.05; **: P<0.01; ***: P<0.001; ****: P<0.0001. Gene identifiers corresponding to Figures A and D are listed in Supplementary Table S2.

and fertility phenotypes, including altered testicular architecture, Leydig cell expansion, reduced mature spermatozoa, and prolonged sperm-release intervals. Together, the data indicate that *hsd3b1* deficiency disrupts testicular endocrine homeostasis and impairs spermatogenic progression.

In the ovaries, 297 DEGs were detected between *hsd3b1*$^{-/-}$ and WT samples, including 149 up-regulated and 148 down-regulated genes (Figure 4D). qPCR validation of selected DEGs confirmed the RNA-seq patterns (Figure 4H). GO enrichment analysis revealed that up-regulated genes were associated with cilium assembly, microtubule cytoskeleton organization, and cell division (Figure 4E). Because cilia and cytoskeletal networks contribute to cellular architecture and morphogenetic regulation (Elkouby & Mullins, 2017; Kikuchi et al., 2024), these changes suggest active early-stage oocyte division and cellular morphology remodeling in *hsd3b1*$^{-/-}$ ovaries. Conversely, genes involved in translation, cellular development, endoplasmic reticulum (ER)-targeting signal recognition particle (SRP), and SRP-dependent membrane protein transport and signal recognition were significantly down-regulated (Figure 4F). The SRP-mediated protein localization pathway is essential for proper membrane protein targeting and organismal viability (Elvekrog & Walter, 2015). As the ER is central to protein folding, processing, and trafficking, down-regulation of these genes suggests reduced transcriptional/translational capacity and impaired protein processing during ovarian development. Integration of transcriptomic profiles with H&E-stained gonadal sections and fertility outcomes indicated that *hsd3b1* deficiency delayed oocyte development and postponed entry into the oocyte maturation stage. Overall, these findings demonstrate that *hsd3b1*$^{-/-}$ zebrafish exhibit delayed gametogenesis in both males and females, while *hsd3b1* knockout does not significantly alter *hsd3b2* expression in testes or ovaries (Supplementary Figure S4B).

hsd3b1 mutants exhibit altered testicular structure

To more precisely define the cellular basis of the altered testicular phenotype, smFISH was performed on WT and *hsd3b1*$^{-/-}$ testes using probes targeting *insl3*, a Leydig cell marker. In WT testes, *insl3*-labeled Leydig cells formed a narrow peripheral layer (Figure 5A1–A3). In contrast, *hsd3b1*$^{-/-}$ testes showed a marked increase in *insl3*-labeled Leydig cells, accompanied by thickening of the cell layer (Figure 5A4–A6). These findings are consistent with the results from H&E staining and transcriptome sequencing. To further assess germ cell development, IF staining was performed on frozen gonadal sections using Piwil1, a germ cell marker that labels spermatogenic cells across developmental stages. Piwil1-positive spermatogenic cells were detected in both WT and *hsd3b1*$^{-/-}$ testes, suggesting that spermatogenic progression was partially preserved despite altered testicular organization (Figure 5B1–B6).

Together, smFISH and histological analyses demonstrated that *hsd3b1* deficiency induced pronounced Leydig cell hyperplasia in zebrafish testes (Figure 3; Figure 5). Despite these structural alterations, Piwil1 immunostaining showed that spermatogenic cells at multiple developmental stages remained present in *hsd3b1*$^{-/-}$ testes (Figure 5). This phenotypic decoupling suggests that germ cell development can persist despite Leydig cell expansion and altered testicular architecture, although the mechanisms supporting residual spermatogenic progression remain to be defined.

hsd3b1 mutants exhibit disrupted steroid hormone metabolism

To define how *hsd3b1* deficiency reshapes the steroid hormone landscape, steroid profiles were quantified in F2 zebrafish at 4 mpf. Four groups were analyzed: WT males (WT_♂), WT females (WT_♀), *hsd3b1*$^{-/-}$ males (−/−_♂), and *hsd3b1*$^{-/-}$ females (−/−_♀), with six zebrafish included in each group (Supplementary Figure S5A).

Figure 6 presents representative steroid hormones that exhibited significant changes and are widely used as clinical indicators of 3β-HSD deficiency; additional steroid measurements are provided in Supplementary Figure S5B–H. 17α-Hydroxyprogesterone was undetectable in WT fish (LOD=0.01 ng/mL) but was detected at low levels in *hsd3b1*$^{-/-}$ females (Figure 6A). Pregnenolone, 17α-hydroxypregnenolone, dehydroepiandrosterone, and 17β-estradiol were present at low levels or below the detection limit in WT fish but were markedly increased in both male and female *hsd3b1*$^{-/-}$ mutants (Figure 6B–D; Supplementary Figure S5B). Androstenedione and testosterone were detected at low concentrations in WT males and females but were elevated in the corresponding *hsd3b1*$^{-/-}$ groups (Figure 6E–F). The persistence of elevated downstream Δ^4-steroids despite loss of *Hsd3b1* suggests partial compensatory steroidogenic activity. Consistent with this possibility, Hsd3b2 enzymatic activity showed an increasing trend in *hsd3b1*$^{-/-}$ mutants (Supplementary Figure S6). In contrast, cortisol and cortisone were significantly reduced relative to WT levels (Figure 6G–H; Supplementary Figure S5C). No significant difference was observed in progesterone levels between *hsd3b1*$^{-/-}$ and WT fish (Supplementary Figure S5D), whereas 11-deoxycortisol, 11-ketotestosterone, and 17α,20β-dihydroprogesterone were reduced in *hsd3b1*$^{-/-}$ males (Supplementary Figure S5G, H). These steroidomic profiles were integrated to summarize the global metabolic consequences of *hsd3b1* deletion in zebrafish (Figure 6I).

Hydrocortisone rescues interrenal tissue hyperplasia in *hsd3b1* mutant embryos

WISH analysis was performed in 5 dpf embryos using an *hsd3b1* probe, with the interrenal tissue-specific marker gene *cyp21a2* used to verify tissue localization (Shi et al., 2022). Results showed that *hsd3b1* expression was concentrated in the interrenal tissue during embryonic development, and *hsd3b1*$^{-/-}$ embryos displayed interrenal tissue hyperplasia (Figure 6J). Because steroid hormone profiling showed a significant reduction in cortisol levels in *hsd3b1*$^{-/-}$ mutants (Figure 6G), exogenous hydrocortisone was administered through the rearing water. Hydrocortisone treatment significantly reduced the expanded interrenal tissue area in *hsd3b1*$^{-/-}$ embryos relative to untreated mutants and restored interrenal size to WT levels (Figure 6J–K). These results indicate that exogenous hydrocortisone administration can rescue the interrenal tissue hyperplasia caused by *hsd3b1* deficiency.

Sexual dimorphism in steroid metabolism is reduced in *hsd3b1* mutants

Steroidomic data were further analyzed to determine whether *hsd3b1* deficiency alters sex-specific endocrine divergence. PCA revealed distinct separation between WT males and females, whereas male and female *hsd3b1*$^{-/-}$ mutants showed a less distinct separation pattern (Supplementary Figure S5A). KEGG analysis of differentially abundant steroid hormones between WT and *hsd3b1*$^{-/-}$ individuals showed that

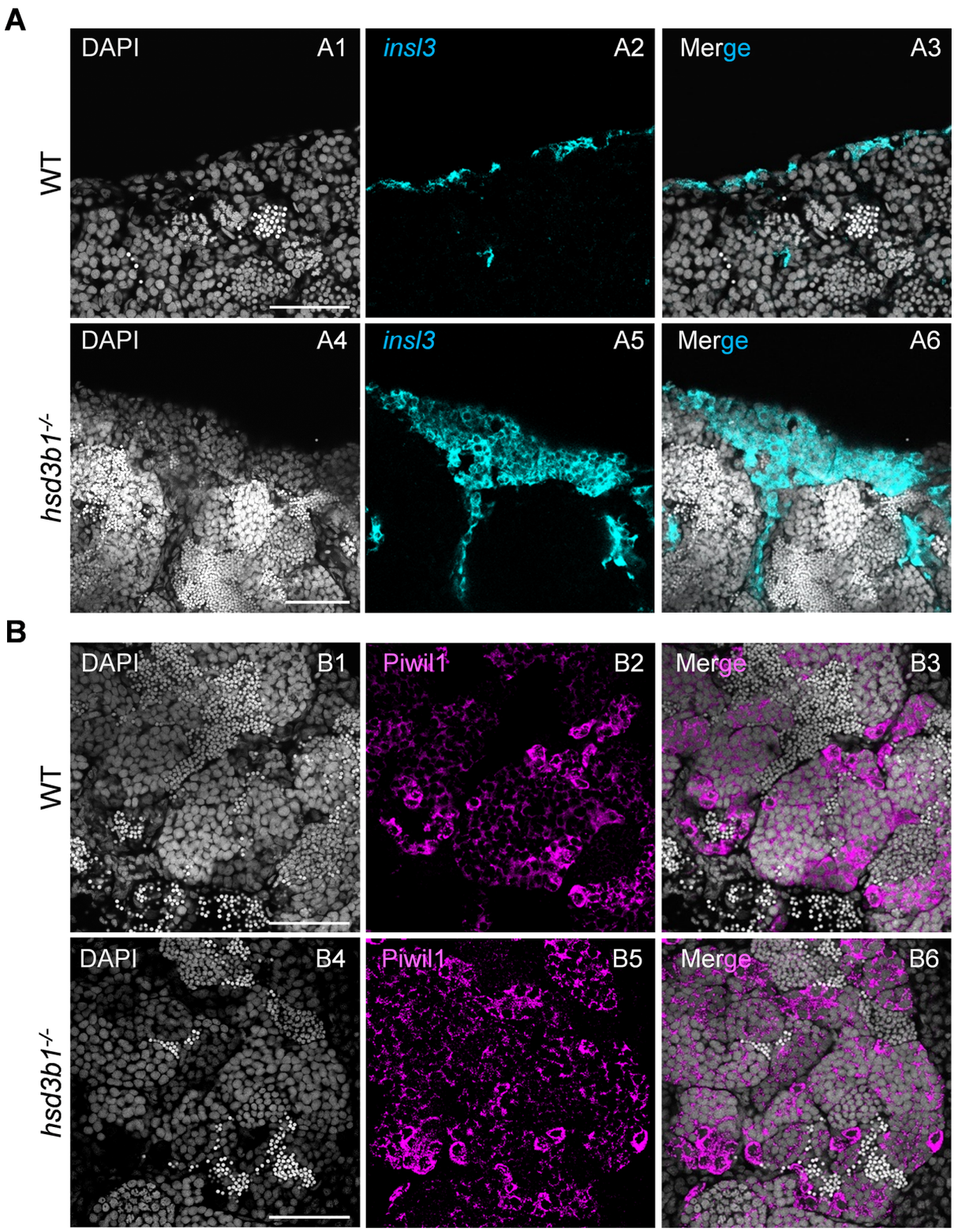


Figure 5 Testicular smFISH and immunofluorescence analysis

A: smFISH analysis of *insl3* expression in testes from 3 mpf WT and *hsd3b1*$^{-/-}$ zebrafish, with DAPI used to counterstain nuclei. Fluorescence signals indicated the distribution of *insl3*-positive Leydig cells in both WT and *hsd3b1*$^{-/-}$ testes. Scale bar: 50 μm. B: Immunofluorescence analysis of Piwil1 expression in testes from 3 mpf WT and *hsd3b1*$^{-/-}$ zebrafish, with DAPI used to counterstain nuclei. Piwil1-positive germ cells were detected in both WT and *hsd3b1*$^{-/-}$ testes. Scale bar: 50 μm.

differences between WT females and males were primarily concentrated in steroid hormone biosynthesis, oocyte maturation and meiosis, and neuroactive ligand-receptor interactions (Figure 7A, C). In contrast, metabolic differences between *hsd3b1*$^{-/-}$ females and males were largely localized to steroid hormone biosynthesis (Figure 7B, D), indicating attenuated sexual dimorphism in steroid metabolism. The decline in progestogens and elevation in androgens appear to confer masculinization characteristics on *hsd3b1*$^{-/-}$ females. Phenotypic traits such as yellowish body coloration and

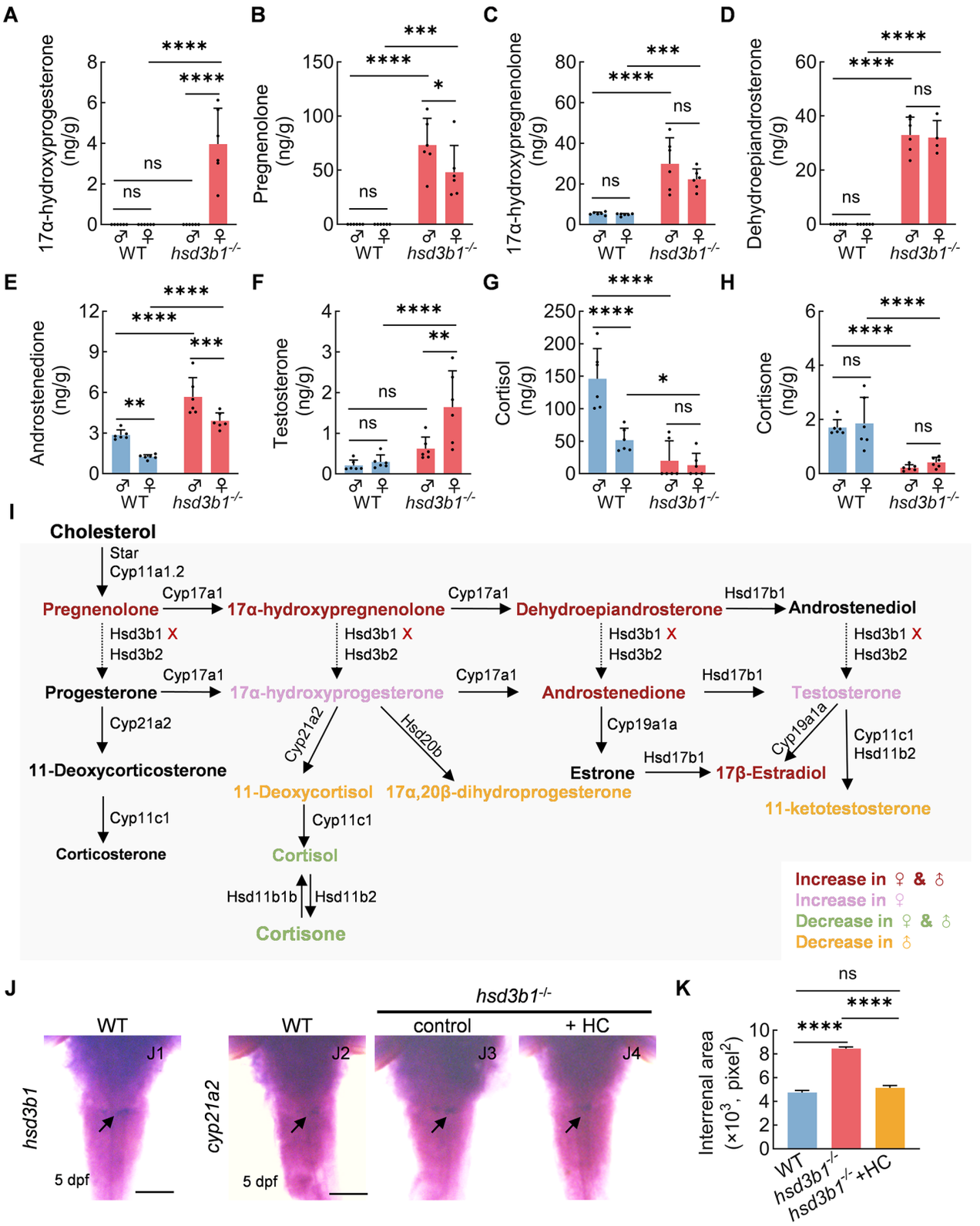


Figure 6 Steroid hormone content and interrenal phenotype in WT and *hsd3b1*$^{-/-}$ zebrafish

A–H: Changes in selected steroid hormone levels in WT and *hsd3b1*$^{-/-}$ zebrafish. Detailed statistical results are provided in Supplementary Tables-S3–S10. I: Global alterations in steroid hormone pathway of *hsd3b1*$^{-/-}$ zebrafish. Hormones shown in dark red increased in both *hsd3b1*$^{-/-}$ females and males; hormones shown in pink increased in *hsd3b1*$^{-/-}$ females; hormones shown in green decreased in both *hsd3b1*$^{-/-}$ females and males; hormones shown in gold decreased in *hsd3b1*$^{-/-}$ males. J: WISH detection of *hsd3b1* or *cyp21a2* expression at 5 dpf. The arrow in the figure indicates the location of the interrenal tissue. J1, *hsd3b1* expression in WT embryos. J2, *cyp21a2* expression in WT embryos. J3, *cyp21a2* expression in *hsd3b1*$^{-/-}$ embryos. J4, *cyp21a2* expression in *hsd3b1*$^{-/-}$ embryos after hydrocortisone treatment. Scale bar: 100 μm. K: Quantification of *cyp21a2*-positive interrenal tissue area in WT, *hsd3b1*$^{-/-}$ control, and *hsd3b1*$^{-/-}$ hydrocortisone-treated embryos. Unit: pixel^2. Data are presented as mean±SD. Two-way analysis of variance was used in panels A–H. Unpaired two-tailed Student's *t*-test was used in panel K. ns: Not significant; *: P<0.05; **: P<0.01; ***: P<0.001; ****: P<0.0001.

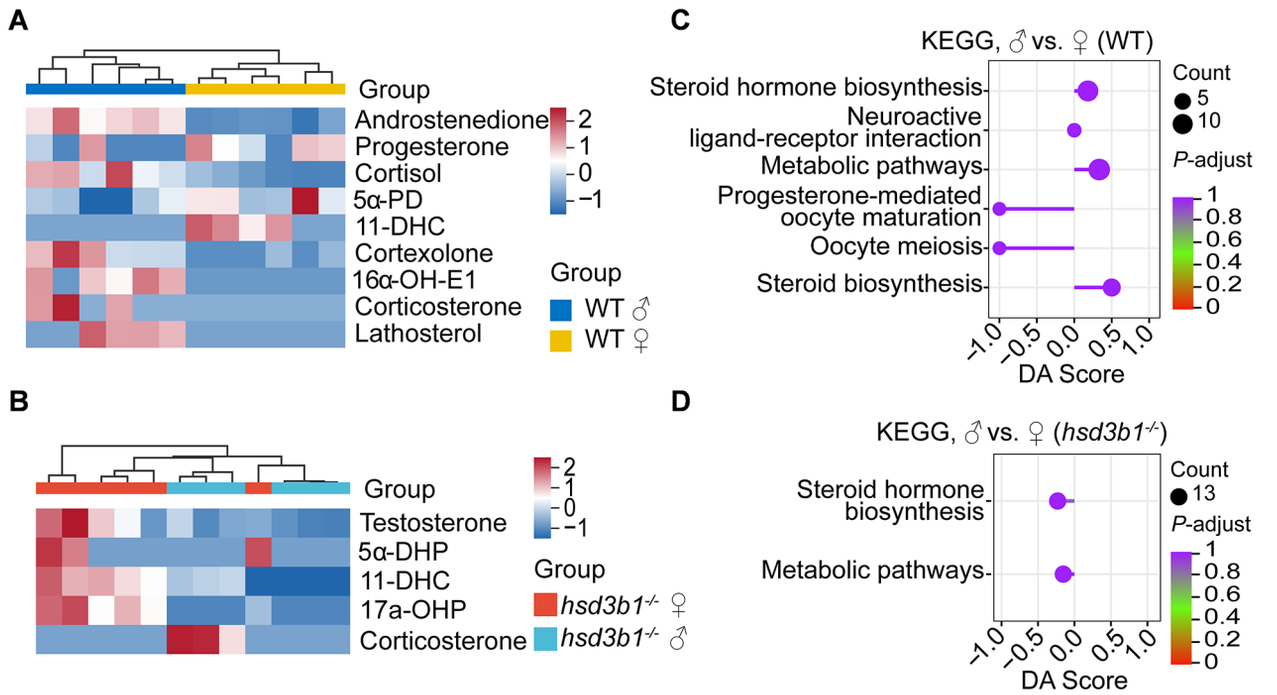


Figure 7 Differential steroid hormone metabolites in WT and *hsd3b1*$^{-/-}$ zebrafish

A: Heatmap of differential steroid hormone metabolites between WT males and females. Abbreviations for selected steroid hormones are as follows: 5α-DHP, 5α-pregnane-3,20-dione; 11-DHC, 11-dehydrocorticosterone; 16α-OH-E1, 16α-hydroxy-estrone; 17-OHP, 17α-hydroxyprogesterone. B: Heatmap of differential steroid hormone metabolites between *hsd3b1*$^{-/-}$ males and females. C: KEGG enrichment analysis of differential steroid hormone metabolic pathways between WT males and females. Differential abundance (DA) score reflects overall metabolite changes within each pathway, with positive values indicating up-regulated metabolites and negative values indicating down-regulated metabolites. Line segment length represents the absolute DA score. D: KEGG enrichment analysis of differential steroid hormone metabolic pathways between *hsd3b1*$^{-/-}$ males and females.

diminished spawning capacity in *hsd3b1*$^{-/-}$ females may be linked to these hormonal changes.

DISCUSSION

This study generated an *hsd3b1*$^{-/-}$ zebrafish line and systematically characterized the multidimensional phenotypic abnormalities caused by *hsd3b1* loss, including disrupted steroid metabolism, altered gonadal development, impaired reproductive capacity, interrenal hyperplasia, and abnormal pigmentation. The mutant phenotype showed multiple parallels with human 3β-HSD deficiency-type CAH caused by loss-of-function mutations in *HSD3B2* (Al Alawi et al., 2019; Auchus, 2022), supporting the value of this zebrafish line as an *in vivo* model for investigating how impaired steroidogenesis affects endocrine and reproductive physiology.

At the morphological level, *hsd3b1*$^{-/-}$ zebrafish exhibited increased body length relative to WT fish. This phenotype resembles accelerated linear growth reported in children with 3β-HSD deficiency, in which altered peripheral steroid metabolism and excess steroid intermediates can promote early somatic growth (Nishi & Tezuka, 1992). Additionally, both male and female *hsd3b1*$^{-/-}$ zebrafish displayed darker body coloration than WT fish, consistent with the hyperpigmentation frequently observed in patients with 3β-HSD deficiency. This pigmentation phenotype is likely linked to impaired cortisol production and compensatory activation of the hypothalamic-pituitary-interrenal axis. Under classical endocrine negative feedback regulation, reduced cortisol levels are expected to stimulate corticotropin-releasing hormone release from the hypothalamus, thereby increasing anterior pituitary synthesis and processing of proopiomelanocortin (POMC) (Shi et al., 2022). POMC gives rise to α-melanocyte-stimulating hormone (α-MSH), adrenocorticotropic hormone (ACTH), and other bioactive peptides, including β-endorphin (Lin & Fisher, 2007). Previous research has shown that *hsd3b1* depletion results in an expanded *pomc* expression domain and increased pigmentation area (Lin et al., 2015). Therefore, increased ACTH and α-MSH production after cortisol depletion provides a plausible mechanistic explanation for the intensified pigmentation observed in *hsd3b1*$^{-/-}$ zebrafish, with α-MSH potentially promoting melanocyte proliferation and melanogenesis.

Reproductive performance was markedly compromised in both male and female *hsd3b1*$^{-/-}$ zebrafish. In females, ovarian development was delayed, as indicated by smaller oocyte diameters at 3 mpf and failure of most mutants to ovulate normally. Although ovulation was partially restored after 5 mpf, egg output remained significantly reduced. This delay in ovarian maturation was closely associated with systemic steroid imbalance caused by *hsd3b1* deficiency. Previous studies have shown that exposure to high concentrations of mixed steroids, including estradiol, progesterone, and androstenedione, can inhibit oocyte maturation (Faltermann et al., 2020), whereas cortisol promotes oocyte maturation and ovulation (Sousa et al., 2015; Zhang et al., 2020b). In *hsd3b1*$^{-/-}$ females, elevated estradiol and androstenedione levels occurred alongside cortisol insufficiency, creating an endocrine environment that likely delayed oocyte maturation and reduced ovulatory competence. Increased ACTH production may further contribute to impaired oocyte development in *hsd3b1*$^{-/-}$ females, given the inhibitory effects

of ACTH on oocyte maturation reported previously (Sousa et al., 2015). In contrast, *hsd3b1* deficiency in males caused pronounced remodeling of testicular architecture. WT testes were almost entirely composed of germ cells, whereas *hsd3b1*$^{-/-}$ testes contained expanded somatic cell populations, primarily Leydig cells, that occupied a substantial proportion of the testicular space. Spermatogenesis in zebrafish follows a cystic pattern, in which cyst-like structures provide the local microenvironment required for coordinated germ cell development (Schulz et al., 2010).Histological and transcriptomic evidence indicated broad disruption of testicular organization in *hsd3b1*$^{-/-}$ males (Figure 3G–L1; Figure 4B), a structural alteration expected to impair spermatogenic efficiency. Leydig cell hyperplasia may represent a secondary response to reduced steroidogenic capacity, potentially mediated by altered endocrine feedback or disrupted intragonadal paracrine signaling. Similar phenotypes have been reported in multiple knockout models targeting steroidogenic enzymes (Wang et al., 2022; Yang et al., 2025), suggesting that impaired steroid biosynthesis is frequently accompanied by expansion of the Leydig cell compartment.

Steroid hormone profiling showed that *hsd3b1*$^{-/-}$ zebrafish of both sexes accumulated Δ^5-3β-hydroxysteroid precursors, including pregnenolone, 17α-hydroxypregnenolone, and dehydroepiandrosterone. This pattern is consistent with impaired 3β-HSD activity, which limits the conversion of these Δ^5 precursors into downstream Δ^4-ketosteroids. Disruption of this early steroidogenic step likely induced compensatory activation of upstream steroid production, thereby promoting substantial precursor accumulation. The concomitant elevation of 17α-hydroxyprogesterone, androstenedione, and testosterone levels indicated that downstream Δ^4-steroid production was not completely abolished, suggesting partial compensation to maintain metabolic processes. Hsd3b2 activity in whole-body extracts showed an increasing trend (Supplementary Figure S6), whereas gonadal transcriptome data showed no significant change in *hsd3b2* expression (Supplementary Figure S4C). These findings suggest that compensation may occur primarily at the enzyme activity level and may involve the participation of extragonadal tissues. The elevated abundance of downstream androgens further indicates that residual or compensatory steroidogenic flux persisted despite *hsd3b1* loss. This pattern is consistent with clinical observations in patients with 3β-HSD deficiency (Guran et al., 2020; Ladjouze et al., 2022). Elevated testosterone may also serve as a precursor for estrogen synthesis, thereby promoting estrogen conversion in peripheral tissues (Burckhardt et al., 2015). Steroid metabolomics further revealed markedly attenuated sexual dimorphism in steroid metabolism in *hsd3b1*$^{-/-}$ mutants, consistent with reduced reproductive performance. In KEGG pathway analysis, differences in oocyte maturation and meiosis pathways were closely associated with impaired ovulation in mutant females. Because steroid hormones play a key role in reproductive endocrine signaling, reduced sex-specific separation in the steroid metabolic profile may disrupt gonadal function and reproductive competence (Cole et al., 2019). However, the present study did not establish a direct causal relationship between individual steroid metabolites and specific reproductive phenotypes.

Testosterone dynamics in *hsd3b1*$^{-/-}$ zebrafish differed significantly from those reported in patients with 3β-HSD deficiency. In male patients, testosterone levels are generally reduced due to insufficient peripheral conversion. In female patients, even limited testosterone production through peripheral conversion can represent relative androgen excess, although testosterone levels may remain within the normal range in mildly affected individuals (Al Alawi et al., 2019). These differences likely reflect fundamental divergence in endocrine anatomy and steroidogenic pathway organization between zebrafish and humans. Specifically, humans possess anatomically distinct adrenal glands with specialized cortical and medullary compartments, and *HSD3B2* is highly expressed in both adrenal and gonadal tissues (Lachance et al., 1991). In contrast, zebrafish lack a discrete adrenal gland; instead, interrenal steroidogenic tissue is distributed only within the head kidney region, and *hsd3b1* expression is most prominent in the testes (Figure 1A; Supplementary Figure S1). Additionally, zebrafish primarily utilize 11-ketotestosterone rather than testosterone as the principal androgen controlling male development (Ogino et al., 2011). These anatomical and metabolic differences may lead to distinct feedback regulatory mechanisms in *hsd3b1*-deficient zebrafish, particularly in males, where *hsd3b1* expression is highest.

Interrenal tissue hyperplasia was also evident in *hsd3b1*$^{-/-}$ zebrafish. Continuous hydrocortisone supplementation through the rearing water effectively reversed this phenotype in *hsd3b1*$^{-/-}$ embryos (Figure 6J–K), confirming the critical role of cortisol replacement in mitigating endocrine abnormalities caused by 3β-HSD deficiency. These findings are consistent with the presence of a negative feedback axis linking cortisol, interrenal steroidogenic tissue, and POMC/ACTH signaling. In *hsd3b1*$^{-/-}$ mutants, impaired steroidogenesis reduced cortisol production, likely relieving feedback inhibition, activating the POMC/ACTH pathway, and promoting interrenal tissue expansion (Ruane et al., 2005). Consistently, hydrocortisone supplementation likely restored feedback inhibition and rescued the hyperplastic phenotype. Based on a previous study (Zhang et al., 2020b), appropriate cortisol supplementation may also support oocyte development in *hsd3b1*$^{-/-}$ females.

In summary, this study demonstrated that *hsd3b1*$^{-/-}$ zebrafish develop endocrine, reproductive, and histopathological abnormalities characteristic of disrupted steroidogenesis, establishing *hsd3b1* as a central regulator of steroid metabolism *in vivo*. This mutant line provides a valuable vertebrate model for exploring how steroidogenic disruption affects development, reproductive physiology, and metabolic processes, and offers a platform for clarifying the pathophysiological mechanisms underlying 3β-HSD deficiency.

DATA AVAILABILITY

The RNA-seq raw data were deposited in the GSA database (PRJCA056249), NCBI database (PRJNA1331710), and Science Data Bank database (https://doi.org/10.57760/sciencedb.35916).

SUPPLEMENTARY DATA

Supplementary data to this article can be found online.

COMPETING INTERESTS

The authors declare that they have no competing interests.

AUTHORS' CONTRIBUTIONS

L.H. designed the research, performed the experiments, analyzed the data, and wrote the manuscript. Y.W., C.W., and R.Q. conducted the experiments. Z.R. designed the research and assisted with the experiments. H.W. and D.Y. assisted with the experiments. Z.C. revised the

figures, provided suggestions, and finalized the manuscript. Y.S. designed the research, analyzed the data, provided suggestions, and finalized the manuscript. All authors read and approved the final version of the manuscript.

ACKNOWLEDGMENTS

We would like to thank other members of the Sun Lab. We would also like to thank Luyuan Pan and Kuoyu Li from the China Zebrafish Resource Center, National Aquatic Biological Resource Center, for assistance with zebrafish husbandry, and Zhixian Qiao, Xiaocui Chai, Fang Zhou, and Guangxin Wang from the Analysis and Testing Center of the Institute of Hydrobiology for technical support.

REFERENCES

Abou Nader N, Boyer A. 2021. Adrenal cortex development and maintenance: knowledge acquired from mouse models. *Endocrinology*, **162**(12): bqab187.

Al Alawi AM, Nordenström A, Falhammar H. 2019. Clinical perspectives in congenital adrenal hyperplasia due to 3β-hydroxysteroid dehydrogenase type 2 deficiency. *Endocrine*, **63**(3): 407–421.

Auchus RJ. 2022. The uncommon forms of congenital adrenal hyperplasia. *Current Opinion in Endocrinology & Diabetes and Obesity*, **29**(3): 263–270.

Auer MK, Nordenström A, Lajic S, et al. 2023. Congenital adrenal hyperplasia. *The Lancet*, **401**(10372): 227–244.

Burckhardt MA, Udhane SS, Marti N, et al. 2015. Human 3β-hydroxysteroid dehydrogenase deficiency seems to affect fertility but may not harbor a tumor risk: lesson from an experiment of nature. *European Journal of Endocrinology*, **173**(5): K1–K12.

Chen LN, Huang HH, Zhang HJ, et al. 2021. Three cases of 3β-hydroxysteroid dehydrogenase deficiency: clinical analysis. *Advances in Clinical and Experimental Medicine*, **30**(3): 289–299.

Chen Z, He M, Wang H, et al. 2024. Intestinal DHA-PA-PG axis promotes digestive organ expansion by mediating usage of maternally deposited yolk lipids. *Nature Communications*, **15**(1): 9769.

Cole TJ, Short KL, Hooper SB. 2019. The science of steroids. *Seminars in Fetal and Neonatal Medicine*, **24**(3): 170–175.

de Castro Assis LH, de Nóbrega RH, Gómez-González NE, et al. 2018. Estrogen-induced inhibition of spermatogenesis in zebrafish is largely reversed by androgen. *Journal of Molecular Endocrinology*, **60**(4): 273–284.

de Waal PP, Leal MC, García-López Á, et al. 2009. Oestrogen-induced androgen insufficiency results in a reduction of proliferation and differentiation of spermatogonia in the zebrafish testis. *Journal of Endocrinology*, **202**(2): 287–297.

Deltourbe LG, Sugrue J, Maloney E, et al. 2025. Steroid hormone levels vary with sex, aging, lifestyle, and genetics. *Science Advances*, **11**(13): eadu6094.

Deng JJ, Xiong F, Ren ZQ, et al. 2026. *cdk2* is essential for synapsis completion and gametogenesis in zebrafish. *Water Biology and Security*, **5**(4): 100532.

Eachus H, Zaucker A, Oakes JA, et al. 2017. Genetic disruption of 21-hydroxylase in zebrafish causes interrenal hyperplasia. *Endocrinology*, **158**(12): 4165–4173.

Elkouby YM, Mullins MC. 2017. Coordination of cellular differentiation, polarity, mitosis and meiosis - New findings from early vertebrate oogenesis. *Developmental Biology*, **430**(2): 275–287.

Elvekrog MM, Walter P. 2015. Dynamics of co-translational protein targeting. *Current Opinion in Chemical Biology*, **29**: 79–86.

Faltermann S, Hettich T, Küng N, et al. 2020. Effects of the glucocorticoid clobetasol propionate and its mixture with cortisol and different class steroids in adult female zebrafish. *Aquatic Toxicology*, **218**: 105372.

Fraga NR, Minaeian N, Kim MS. 2024. Congenital adrenal hyperplasia. *Pediatrics in Review*, **45**(2): 74–84.

Gonzalez Deniselle MC, Liere P, Pianos A, et al. 2016. Steroid profiling in male wobbler mouse, a model of amyotrophic lateral sclerosis. *Endocrinology*, **157**(11): 4446–4460.

Gotoh H, Kusakabe M, Shiroishi T, et al. 1994. Survival of steroid 21-hydroxylase-deficient mice without endogenous corticosteroids after neonatal treatment and genetic rescue by transgenesis as a model system for treatment of congenital adrenal hyperplasia in humans. *Endocrinology*, **135**(4): 1470–1476.

Gotoh H, Sagai T, Hata JI, et al. 1988. Steroid 21-hydroxylase deficiency in mice. *Endocrinology*, **123**(4): 1923–1927.

Guran T, Kara C, Yildiz M, et al. 2020. Revisiting classical 3β-hydroxysteroid dehydrogenase 2 deficiency: lessons from 31 pediatric cases. *The Journal of Clinical Endocrinology & Metabolism*, **105**(3): e1718–e1728.

Ikeda Y, Shen WH, Ingraham HA, et al. 1994. Developmental expression of mouse steroidogenic factor-1, an essential regulator of the steroid hydroxylases. *Molecular Endocrinology*, **8**(5): 654–662.

Ivell R, Wade JD, Anand-Ivell R. 2013. INSL3 as a biomarker of Leydig cell functionality. *Biology of Reproduction*, **88**(6): 147.

Kanehisa M, Goto S. 2000. KEGG: kyoto encyclopedia of genes and genomes. *Nucleic Acids Research*, **28**(1): 27–30.

Kikuchi M, Yoshimoto M, Ishikawa T, et al. 2024. Sexually dimorphic dynamics of the microtubule network in medaka (*Oryzias latipes*) germ cells. *Development*, **151**(5): dev201840.

Kimmel CB, Ballard WW, Kimmel SR, et al. 1995. Stages of embryonic development of the zebrafish. *Developmental Dynamics*, **203**(3): 253–310.

Lachance Y, Luu-The V, Verreault H, et al. 1991. Structure of the human type II 3β-hydroxysteroid dehydrogenase/Δ^5-Δ^4 isomerase (3β-HSD) gene: adrenal and gonadal specificity. *DNA and Cell Biology*, **10**(10): 701–711.

Ladjouze A, Donaldson M, Plotton I, et al. 2022. Genotype, mortality, morbidity, and outcomes of 3β-hydroxysteroid dehydrogenase deficiency in algeria. *Frontiers in Endocrinology*, **13**: 867073.

Lau ESW, Zhang ZW, Qin MM, et al. 2016. Knockout of zebrafish ovarian aromatase gene (*cyp19a1a*) by TALEN and CRISPR/Cas9 leads to all-male offspring due to failed ovarian differentiation. *Scientific Reports*, **6**(1): 37357.

Li N, Oakes JA, Storbeck KH, et al. 2020. The P450 side-chain cleavage enzyme Cyp11a2 facilitates steroidogenesis in zebrafish. *Journal of Endocrinology*, **244**(2): 309–321.

Li WH, Li ZQ, Bu MD, et al. 2024a. Metabolomic-based analysis reveals bile acid-mediated ovarian failure induced by low temperature in zebrafish. *Zoological Research*, **45**(4): 791–804.

Li Y, Li XH, Ye D, et al. 2024b. Endogenous biosynthesis of docosahexaenoic acid (DHA) regulates fish oocyte maturation by promoting pregnenolone production. *Zoological Research*, **45**(1): 176–188.

Lin JC, Hu S, Ho PH, et al. 2015. Two zebrafish *hsd3b* genes are distinct in function, expression, and evolution. *Endocrinology*, **156**(8): 2854–2862.

Lin JY, Fisher DE. 2007. Melanocyte biology and skin pigmentation. *Nature*, **445**(7130): 843–850.

Love MI, Huber W, Anders S. 2014. Moderated estimation of fold change and dispersion for RNA-seq data with DESeq2. *Genome Biology*, **15**(12): 550.

Luzio A, Monteiro SM, Garcia-Santos S, et al. 2015. Zebrafish sex differentiation and gonad development after exposure to 17α-ethinylestradiol, fadrozole and their binary mixture: a stereological study. *Aquatic Toxicology*, **166**: 83–95.

Mermejo LM, Elias LLK, Marui S, et al. 2005. Refining hormonal diagnosis of type II 3β-hydroxysteroid dehydrogenase deficiency in patients with premature pubarche and hirsutism based on HSD3B2 genotyping. *The Journal of Clinical Endocrinology & Metabolism*, **90**(3): 1287–1293.

Miller WL, Auchus RJ. 2011. The molecular biology, biochemistry, and physiology of human steroidogenesis and its disorders. *Endocrine Reviews*,

32(1): 81–151.

Moisan AM, Ricketts ML, Tardy V, et al. 1999. New insight into the molecular basis of 3beta-hydroxysteroid dehydrogenase deficiency: identification of eight mutations in the *HSD3B2* gene eleven patients from seven new families and comparison of the functional properties of twenty-five mutant enzymes. *The Journal of Clinical Endocrinology & Metabolism*, **84**(12): 4410–4425.

Moreno-Mateos MA, Vejnar CE, Beaudoin JD, et al. 2015. CRISPRscan: designing highly efficient sgRNAs for CRISPR-Cas9 targeting *in vivo*. *Nature Methods*, **12**(10): 982–988.

Naiki Y, Miyado M, Horikawa R, et al. 2016. Extra-adrenal induction of *Cyp21a1* ameliorates systemic steroid metabolism in a mouse model of congenital adrenal hyperplasia. *Endocrine Journal*, **63**(10): 897–904.

Nishi Y, Tezuka T. 1992. Mild adrenal 3β-hydroxysteroid dehydrogenase deficiency in children with accelerated growth, premature pubarche and/or hirsutism. *European Journal of Pediatrics*, **151**(1): 19–23.

Nouri MZ, Kroll KJ, Webb M, et al. 2020. Quantification of steroid hormones in low volume plasma and tissue homogenates of fish using LC-MS/MS. *General and Comparative Endocrinology*, **296**: 113543.

Ogino Y, Miyagawa S, Katoh H, et al. 2011. Essential functions of androgen signaling emerged through the developmental analysis of vertebrate sex characteristics. *Evolution & Development*, **13**(3): 315–325.

Ren ZQ, Ye D, Su N, et al. 2024. *foxl2l* is a germ cell-intrinsic gatekeeper of oogenesis in zebrafish. *Zoological Research*, **45**(5): 1116–1130.

Ruane NM, Lambert JGD, Goos HJT, et al. 2005. Hypocorticism and interrenal hyperplasia are not directly related to masculinization in XX *mas*$^{-1}$/*mas*$^{-1}$ carp, *Cyprinus carpio*. *General and Comparative Endocrinology*, **143**(1): 66–74.

Schulz RW, de França LR, Lareyre JJ, et al. 2010. Spermatogenesis in fish. *General and Comparative Endocrinology*, **165**(3): 390–411.

Secchi C, Belli M, Harrison TNH, et al. 2021. Effect of the spatial-temporal specific theca cell Cyp17 overexpression on the reproductive phenotype of the novel TC17 mouse. *Journal of Translational Medicine*, **19**(1): 428.

Shi SC, Shu TT, Li X, et al. 2022. Characterization of the interrenal gland and sexual traits development in *cyp17a2*-deficient zebrafish. *Frontiers in Endocrinology*, **13**: 910639.

Simard J, Moisan AM, Morel Y. 2002. Congenital adrenal hyperplasia due to 3β-hydroxysteroid dehydrogenase/Δ^5-Δ^4 isomerase deficiency. *Seminars in Reproductive Medicine*, **20**(3): 255–276.

Simard J, Ricketts ML, Gingras S, et al. 2005. Molecular biology of the 3β-hydroxysteroid dehydrogenase/Δ^5-Δ^4 isomerase gene family. *Endocrine Reviews*, **26**(4): 525–582.

Sousa ML, Figueiredo F, Pinheiro C, et al. 2015. Morphological and molecular effects of cortisol and ACTH on zebrafish stage I and II follicles. *Reproduction*, **150**(5): 429–436.

Su NK, Ren ZQ, Wang HP, et al. 2026. Cyprinid Juji (*Gobiocypris rarus*) as a model fish to study germ cell development and gonadal differentiation. *Communications Biology*, **9**(1): 106.

Tang HP, Chen Y, Liu Y, et al. 2017. New insights into the role of estrogens in male fertility based on findings in aromatase-deficient zebrafish. *Endocrinology*, **158**(9): 3042–3054.

Thisse C, Thisse B. 2008. High-resolution *in situ* hybridization to whole-mount zebrafish embryos. *Nature Protocols*, **3**(1): 59–69.

Tong ZB, Otsuka N, Tu W, et al. 2022. P450 side-chain cleavage enzyme (P450-SCC) is an ovarian autoantigen in a mouse model for autoimmune oophoritis. *Reproductive Sciences*, **29**(8): 2391–2400.

Uribe MC, Grier HJ, Mejía-Roa V. 2014. Comparative testicular structure and spermatogenesis in bony fishes. *Spermatogenesis*, **4**(3): e983400.

Wang XS, Zhu JW, Wang HP, et al. 2023. Induced formation of primordial germ cells from zebrafish blastomeres by germplasm factors. *Nature Communications*, **14**(1): 7918.

Wang YQ, Ye D, Zhang FH, et al. 2022. *Cyp11a2* is essential for oocyte development and spermatogonial stem cell differentiation in zebrafish. *Endocrinology*, **163**(2): bqab258.

Waterhouse A, Bertoni M, Bienert S, et al. 2018. SWISS-MODEL: homology modelling of protein structures and complexes. *Nucleic Acids Research*, **46**(W1): W296–W303.

Watters RJ, Verdelis K, Lucas PC, et al. 2021. A novel mouse model for SNP in steroid receptor co-activator-1 reveals role in bone density and breast cancer metastasis. *Endocrinology*, **162**(8): bqab094.

Wu K, Song WY, Zhang ZW, et al. 2020. Disruption of *dmrt1* rescues the all-male phenotype of the cyp19a1a mutant in zebrafish – a novel insight into the roles of aromatase/estrogens in gonadal differentiation and early folliculogenesis. *Development*, **147**(4): dev182758.

Wu TZ, Hu EQ, Xu SB, et al. 2021. clusterProfiler 4.0: a universal enrichment tool for interpreting omics data. *The Innovation*, **2**(3): 100141.

Yang LY, Wu Y, Du YY, et al. 2025. Dual *cyp17a1/a2* knockout unveils paralog-specific steroid pathways in fish reproduction. *International Journal of Biological Macromolecules*, **316**: 144772.

Yang LY, Wu Y, Zhang XF, et al. 2024. Investigating the molecular mechanisms of oocyte maturation and ovulation in Nile tilapia: a focus on the steroidogenic enzyme Cyp17a2. *Zoological Research*, **45**(6): 1357–1370.

Yang LY, Zhang XF, Liu SJ, et al. 2021. Cyp17a1 is required for female sex determination and male fertility by regulating sex steroid biosynthesis in fish. *Endocrinology*, **162**(12): bqab205.

Ye D, Liu T, Li YM, et al. 2023. Identification of fish spermatogenic cells through high-throughput immunofluorescence against testis with an antibody set. *Frontiers in Endocrinology*, **14**: 1044318.

Yin YK, Tang HP, Liu Y, et al. 2017. Targeted disruption of aromatase reveals dual functions of *cyp19a1a* during sex differentiation in zebrafish. *Endocrinology*, **158**(9): 3030–3041.

Zhai G, Shu TT, Xia YG, et al. 2018. Characterization of sexual trait development in *cyp17a1*-deficient zebrafish. *Endocrinology*, **159**(10): 3549–3562.

Zhang FH, Li XM, He MD, et al. 2020a. Efficient generation of zebrafish maternal-zygotic mutants through transplantation of ectopically induced and Cas9/gRNA targeted primordial germ cells. *Journal of Genetics and Genomics*, **47**(1): 37–47.

Zhang QF, Ye D, Wang HP, et al. 2020b. Zebrafish *cyp11c1* Knockout Reveals the Roles of 11-ketotestosterone and Cortisol in Sexual Development and Reproduction. *Endocrinology*, **161**(6): bqaa048.

Zhang R, Jiao SB, He MD, et al. 2025. An oocyte and yolk syncytial layer-derived Nanog-*cyp11a1*-pregnenolone axis promotes extraembryonic development. *Science Bulletin*, **70**(24): 4150–4155.

Zhang YK, Jiang YJ, Sun Q, et al. 2024. Full sexual maturity-cycle exposure to environmentally relevant concentrations of 17β-estradiol decreases reproductive capacity of zebrafish. *Journal of Environmental Sciences*, **137**: 580–592.

Zhang ZG, Coutinho AE, Man TY, et al. 2017. Macrophage 11β-HSD-1 deficiency promotes inflammatory angiogenesis. *Journal of Endocrinology*, **234**(3): 291–299.

Zhou LY, Li MH, Wang DS. 2021. Role of sex steroids in fish sex determination and differentiation as revealed by gene editing. *General and Comparative Endocrinology*, **313**: 113893.

Zirkin BR, Papadopoulos V. 2018. Leydig cells: formation, function, and regulation. *Biology of Reproduction*, **99**(1): 101–111.